Note

Vibrational spectroscopy of N_2O in solid neon matrices

Lei Wan, Gang Xu, Lei Wu, Yang Chen, Shui-Ming Hu *

Hefei National Laboratory for Physical Sciences at Microscale, University of Science and Technology of China, Hefei 230026, China

Since nitrous oxide is a very important green house molecule and often used as a reagent in photolysis dynamics studies, the spectra of nitrous oxide have been extensively studied. The matrix isolation spectroscopy have been reported for N_2O in solid N_2 [1–3], Ar [3–6], Xe [6,7], *para* hydrogen [8,9] and also in Helium droplet [10]. The spectrum of ^4He_n-N_2O ($n = 2$–20) clusters was also reported in Ref. [11]. The matrix shift and matrix splitting observed in different matrices provide a measure of the intermolecular interactions between the host and guest molecules. The matrix shift ranges from 5 to 12 cm^{-1} for the v_3 band of N_2O in heavy rare-gas and N_2 matrices while much less in Helium droplet and in solid *para* H_2. The strong fundamental bands of N_2O were extensively studied in the literature, but the overtones are less considered because such bands are much weaker and often hard to be identified from the bands of other contaminations in the sample. In the present work, the infrared spectra of the N_2O molecules embedded in neon are investigated, from the strong fundamental bands to the much weaker overtones extended to the 2 μm region. The vibrational assignments are confirmed by a systematic study of different isotopologues of N_2O.

Three commercial N_2O samples were used in the present study, one was natural sample (containing 99% $^{14}N_2^{16}O$) bought from Nanjing Special Gas Co., other two are ^{15}N enriched samples purchased from Icon Services Inc. Concluded from the infrared spectroscopy and the mass spectroscopy measurements, one ^{15}N enriched sample was with 99% $^{15}N^{14}N^{16}O$ and the other one was with 97% $^{14}N^{15}N^{16}O$. These three samples will be noted below as N_2O-446, N_2O-546 and N_2O-456, respectively. In the premixed N_2O/Ne sample, the concentra-

tion of N_2O was about 500 ppm. The N_2O/Ne sample was deposited on a BaF_2 substrate through a 0.1 mm diameter pinhole. The distance between the pinhole and the BaF_2 substrate was about 3 cm. The flow rate was controlled at about 1 mmol/min by a mass-flow controller. The BaF_2 substrate was attached to the cold head of a closed-cycle cryostat (Janis SHI-4-5). A LakeShore 331S controller was used to control the heating current in a wire attached to the cold head. In this way, the temperature can be adjusted in the range of 3.5–20 K with 0.2 K accuracy. In the measurements, the premixed N_2O/Ne samples were deposited at 4.4 K and then annealed at 8 K for 30 min. The infrared absorption spectra were recorded by a Bruker IFS120HR FT-IR spectrometer. The infrared light beam passed the cold BaF_2 substrate with a 45° angle. The entire optical path was evacuated to avoid the atmospheric absorption. The spectra covering the ranges 700–6000 cm^{-1} were recorded with proper selections of the light sources (glowbar or tungsten lamp), beam splitters (KBr or CaF$_2$) and detectors (lN$_2$ cooled MCT or InSb). The adopted spectral resolution was 0.02 cm^{-1}.

In addition to the very strong v_3 bands of $^{14}N^{14}N^{16}O$, $^{14}N^{15}N^{16}O$ and $^{15}N^{14}N^{16}O$, many overtones were observed when more sample gas was deposited. The bands can be assigned according to the band centers of N_2O in gas phase available in Refs. [12–14]. The comparison of the spectra of the samples with different isotopic abundances also helped us to identify the N_2O overtones from other weak lines due to minor contaminant molecules (like water) in the sample. All the band shift values respect to the corresponding upper vibrational state energies in gas phase are given in Table 1. It can be easily found that the matrix shift values have a quite linear

---

Table 1
Matrix shifts of the vibrational bands of N_2O in neon (in cm^{-1})

Band[a]	Isotope[b]	G_v[c]	Δv[d]	δ_{Calc}[e]	I_{exp}[f]
02^00	456	1144.3334	3.36	3.58	5.4E − 3
	546	1159.9717	3.50	3.40	1.9E − 2
	446	1168.1323			
10^00	456	1280.3541	0.39	0.56	3.1E − 1
	546	1269.8920	0.68	0.96	2.1E − 1
	446	1284.9033	0.58	0.83	2.6E − 1
00^01	556	2154.7259	1.43		
	458	2171.0442	1.48		
	548	2194.0456	1.50		
	547	2197.6486	1.54		
	448	2216.7112	1.53		
	456	2177.6568	1.47	1.52	1
	546	2201.6053	1.47	1.55	1
	446	2223.7568	1.50	1.57	1
04^00	456	2278.1927			
	546	2305.1626	6.63	6.79	1.4E − 3
	446	2322.5731	6.66	6.85	2.6E − 4
12^00	456	2431.3225	4.10	4.14	3.8E − 3
	546	2439.6246	4.37	4.35	1.0E − 2
	446	2461.9964	4.29	4.25	1.1E − 2
20^00	456	2552.4082	0.97	1.12	4.4E − 2
	546	2534.5321	1.75	1.91	4.1E − 2
	446	2563.3394	1.45	1.65	4.7E − 2
01^11	456	2739.5981	3.17[g]	3.31	4.7E − 3
	546	2772.7027	3.42[g]	3.25	9.2E − 4
	446	2798.2926	3.41[g]	3.29	3.1E − 3
02^01	456	3295.4621	5.12	5.10	7.8E − 4
	546	3333.7393	5.23	4.95	4.4E − 3
	446	3363.9780	5.25	5.00	2.1E − 3
10^01	456	3432.1931	2.03	2.08	6.1E − 2
	546	3443.6500	2.25	2.51	6.7E − 2
	446	3480.8192	2.19	2.40	7.6E − 2
22^00	456	3709.8128	5.00	4.70	3.0E − 4
	546	3712.1285	5.15	5.31	1.8E − 3
	446	3748.2518	5.11	5.08	2.0E − 3
30^00	456	3816.4754	1.68	1.69	1.7E − 3
	546	3795.4509	3.29	2.87	1.7E − 3
	446	3836.3710	2.78	2.48	1.3E − 3
00^02	456	4326.6172	3.15	3.04	2.0E − 3
	546	4373.6061	3.06	3.10	5.5E − 4
	446	4417.3778	3.14	3.15	1.4E − 3
20^01	456	4677.7978	2.64	2.64	1.3E − 3
	546	4679.9182	3.42	3.46	9.2E − 4
	446	4730.8250	3.16	3.23	4.4E − 4

[a] Quantum numbers of the upper states, $V_1 V_2^{l_2} V_3$.
[b] Index of different isotopologues of N_2O, 446: $^{14}N\ ^{14}N\ ^{16}O$, 456: $^{14}N^{15}N^{16}O$, 546: $^{15}N^{14}N^{16}O$, and so on.
[c] Gas phase values, adopted from Refs. [12,13].
[d] Experimental neon matrix shift, $\Delta v = v_{Matrix} - G_v$.
[e] Matrix shift calculated with parameters in Table 2 following Eq. (1).
[f] Relative integrated band intensity, respect to the v_3 band for each isotopologue.
[g] Band consisted of two lines separated with 1.2 cm^{-1}, shown in Fig. 2.

dependence on the vibrational quantum numbers. They can be interpreted very well in the form:

$$\Delta v(V_1, V_2, V_3) = v_{matrix} - G_v = \alpha_1 V_1 + \alpha_2 V_2 + \alpha_3 V_3 \quad (1)$$

Table 2
Coefficients used to reproduce the band shifts of N_2O/Ne, see Eq. (1), in cm^{-1}

	$^{14}N^{15}N^{16}O$	$^{15}N^{14}N^{16}O$	$^{14}N^{14}N^{16}O$
α_1	0.56	0.96	0.83
α_2	1.79	1.70	1.71
α_3	1.52	1.55	1.57
σ[a]	0.14	0.22	0.18

[a] σ is the rms of the least-square fitting.

where V_i $(i = 1, 2, 3)$ are the vibrational quantum numbers of the upper vibrational state, Δv is the neon matrix shift of the band, α_i $(i = 1, 2, 3)$ are the corresponding coefficients. For N_2O-446, 456 and 546 isotopologues, we can get the α values from least-squares fitting of the observed matrix shifts Δv given in Table 1. The fitted α values and the root-mean-squares of the fitting are presented in Table 2. For each of the isotopologues, a set of three parameters can reproduce the observed band shifts with the accuracy of about 0.2 cm^{-1}. For comparison, the calculated neon matrix shifts are also given in Table 1. In the table, we also give the experimental relative integrated band intensities. Note the values were scaled to the respective v_3 band values for each isotopologue.

Most of the observed N_2O/Ne bands do not show detectable structures at our experimental resolution (0.02 cm^{-1}). Each band just has a band width (Full Width at Half Maximum) about 0.1–0.3 cm^{-1}. For illusion, the nv_1 $(n = 1, 2, 3)$ bands of $^{15}N^{14}N^{16}O$ and $nv_1 + v_3$ $(n = 0, 1, 2)$ bands of $^{14}N_2^{16}O$ are presented in Fig. 1. Note that both of the observed band shifts and band widths are relatively much smaller than those observed in other rare-gas matrices.

It is interesting to address that for the band shown in Fig. 2, which is near 2798 cm^{-1} for N_2O-446 and near 2773 cm^{-1} for N_2O-546, the band is consisted of two peaks with comparable intensities, separated with 1.2 cm^{-1}. Since the same structures were observed for different N_2O isotopologues with respective frequency shifts very close to that predicted by Eq. (1), we assigned them to the $01^11 \leftarrow 00^00$ bands of respective N_2O isotopologues. The splitting can be a result of the multi-orientation sites of N_2O in the neon matrix, but it remains unknown to us that why only this band has such splitting structure while not for any other bands observed in this work.
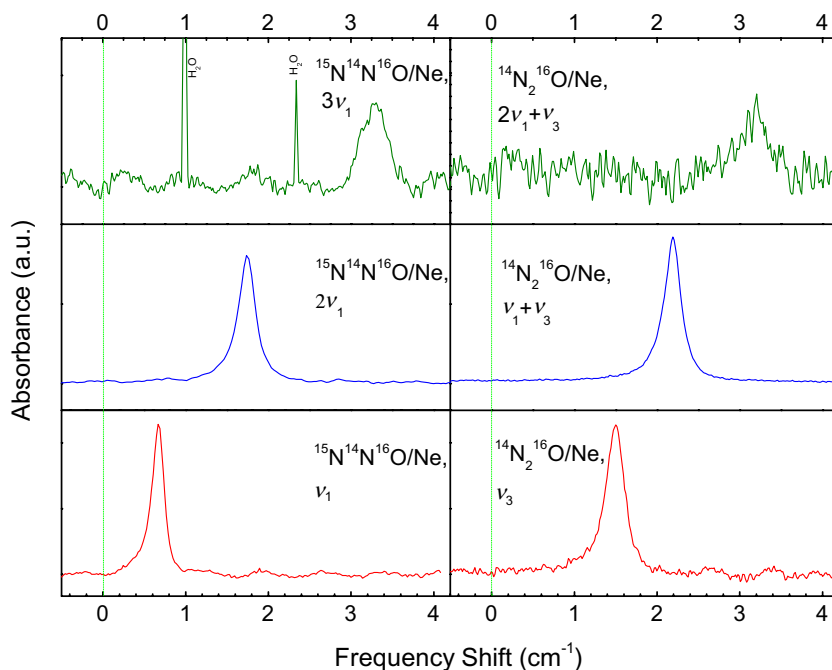
Fig. 1. The v_1, $2v_1$ and $3v_1$ bands of $^{15}N^{14}N^{16}O/Ne$ (left panel) and the v_3, $v_1 + v_3$ and $2v_1 + v_3$ bands of $^{14}N^{14}N^{16}O/Ne$ (right panel). The frequency shifts given on the figure are respect to the gas phase G_v values given in Table 1 of each isotopologue. The relative band intensity values are given in Table 1.
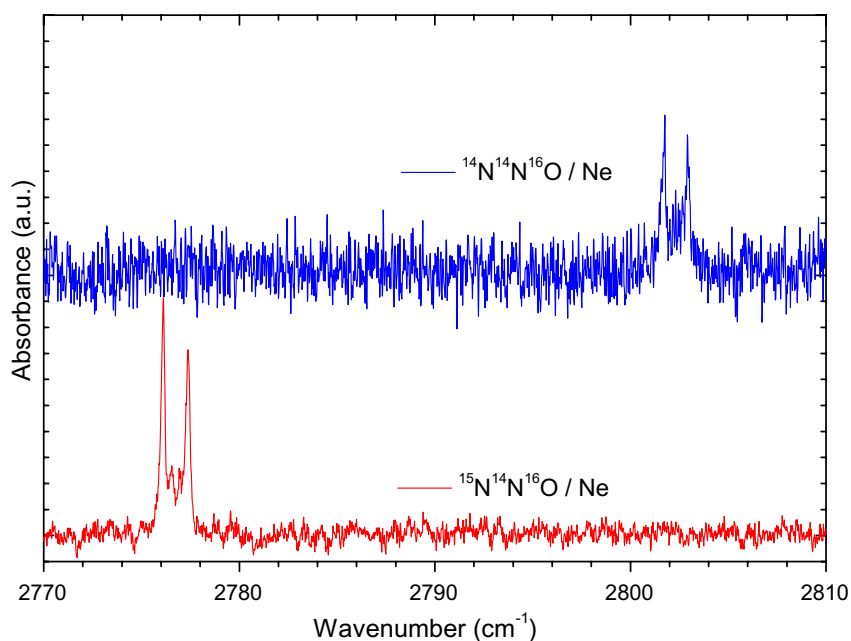

Fig. 2. $v_2 + v_3$ band of $^{14}N^{14}N^{16}O$ (upper) and $^{15}N^{14}N^{16}O$ (lower) in neon matrices. The band has two splitting peaks separated with 1.2 cm^{-1}.

References

[1] M. Bahou, L. Schriver-Mazzuoli, C. Camy-Peyret, A. Schriver, J. Chem. Phys. 108 (1998) 6884–6891.

[2] A. Łapiński, J. Spanget-Larsen, J. Waluk, J.G. Radziszewski, J. Chem. Phys. 115 (2001) 1757–1764.

[3] L.M. Nxumalo, T.A. Ford, J. Mol. Struct. 327 (1994) 145–159.

[4] H. Chabbi, P.R. Dahoo, B. Gauthier-Roy, A.-M. Vasserot, L. Abouaf-Marguin, J. Phys. Chem. A104 (2000) 1670–1673.

[5] S. Kudoh, K. Onoda, M. Takayanagi, M. Nakata, J. Mol. Struct. 524 (2000) 61–68.

[6] W.G. Lawrence, V.A. Apkarian, J. Chem. Phys. 97 (1992) 2224–2228.

[7] H. Krueger, E. Weitz, J. Chem. Phys. 96 (1992) 2846–2855.

[8] K. Yoshioka, P.L. Raston, D.T. Anderson, Int. Rev. Phys. Chem. 25 (2006) 469–496.

[9] B.D. Lorenz, D.T. Anderson, J. Chem. Phys. 126 (2007) 184506.

[10] K. Nauta, R.E. Miller, J. Chem. Phys. 115 (2001) 10254–10260.

[11] Yunjie Xu, Wolfgang Jäger, Jian Tang, A.R.W. McKellar, Phys. Rev. Lett. 91 (2003) 163401.

[12] R.A. Toth, Appl. Opt. 30 (1991) 5289–5315.

[13] R.A. Toth, J. Mol. Spectrosc. 197 (1999) 158–187.

[14] H.-Y. Ni, K.-F. Song, V.I. Perevalov, S.A. Tashkun, A.-W. Liu, L. Wang, S.-M. Hu, J. Mol. Spectrosc. 248 (2008) 41–60.